J. Fluid Mech. (2015), *vol.* 786, *pp.* 234–252.
doi:10.1017/jfm.2015.664

On the universality of local dissipation scales in turbulent channel flow

S. C. C. Bailey[1,†] **and B. M. Witte**[1]

[1]Department of Mechanical Engineering, University of Kentucky, Lexington, KY 40506, USA

(Received 10 December 2014; revised 11 September 2015; accepted 4 November 2015)

Well-resolved measurements of the small-scale dissipation statistics within turbulent channel flow are reported for a range of Reynolds numbers from $Re_\tau \approx 500$ to 4000. In this flow, the local large-scale Reynolds number based on the longitudinal integral length scale is found to poorly describe the Reynolds number dependence of the small-scale statistics. When a length scale based on Townsend's attached-eddy hypothesis is used to define the local large-scale Reynolds number, the Reynolds number scaling behaviour was found to be more consistent with that observed in homogeneous, isotropic turbulence. The Reynolds number scaling of the dissipation moments up to the sixth moment was examined and the results were found to be in good agreement with predicted scaling behaviour (Schumacher *et al.*, *Proc. Natl Acad. Sci. USA*, vol. 111, 2014, pp. 10961–10965). The probability density functions of the local dissipation scales (Yakhot, *Physica* D, vol. 215 (2), 2006, pp. 166–174) were also determined and, when the revised local large-scale Reynolds number is used for normalization, provide support for the existence of a universal distribution which scales differently for inner and outer regions.

Key words: turbulence theory, turbulent boundary layers, turbulent flows

1. Introduction

One of the most significant milestones in the study of turbulence is the classical theory presented by Kolmogorov (1941). A cornerstone of this theory is the assumption that the small scales of turbulence are homogeneous and isotropic. Furthermore, these smallest scales are assumed to demonstrate universal characteristics which depend only on the mean rate of dissipation of the turbulent kinetic energy, $\langle\varepsilon\rangle$, and the kinematic viscosity, ν. Thus leading to the definition of the Kolmogorov length scale, $\eta_K \sim (\nu^3/\langle\varepsilon\rangle)^{1/4}$. A great body of evidence has been produced to support Kolmogorov's concept of small-scale universality, particularly through collapse of the high-wavenumber portion of the energy spectrum scaled using ν, $\langle\varepsilon\rangle$ and η_K (i.e. Grant, Stewart & Moilliet 1962; Saddoughi & Veeravalli 1994).

In Kolmogorov's theory, the average flux of energy from the turbulent-kinetic-energy-producing turbulence, characterized by length scale L, down to the smallest scales, characterized by η_K, is equal to $\langle\varepsilon\rangle$ for sufficient separation of L and η_K. Here,

† Email address for correspondence: sean.bailey@uky.edu

$\langle\,\rangle$ describes an ensemble-averaged quantity and $\langle\varepsilon\rangle$ can be found by averaging the instantaneous dissipation rate of turbulent kinetic energy

$$\varepsilon = \frac{\nu}{2}\left(\frac{\partial u_i}{\partial x_j} + \frac{\partial u_j}{\partial x_i}\right)\left(\frac{\partial u_i}{\partial x_j} + \frac{\partial u_j}{\partial x_i}\right), \tag{1.1}$$

where t is time, u_i represents the fluctuating components of the velocity vector such that $u_i(\boldsymbol{x}, t) = U_i(\boldsymbol{x}, t) - \langle U_i(\boldsymbol{x}, t)\rangle$ with U_i the components of the instantaneous local velocity vector. Within the inertial subrange, in which the spatial separation represented by vector $\boldsymbol{r}$ is in the range $L \gg |\boldsymbol{r}| \gg \eta_K$, the longitudinal structure functions, S_n are predicted to follow power law behaviour such that

$$S_n \equiv \langle(\delta_r u)^n\rangle = A_n\left(\frac{|\boldsymbol{r}|}{L}\right)^{\zeta_n}, \tag{1.2}$$

where $\delta_r u$ is the longitudinal velocity increment defined as

$$\delta_r u = (u_i(x_j + r_j) - u_i(x_j))\left(\frac{r_i}{|\boldsymbol{r}|}\right). \tag{1.3}$$

According to Kolmogorov's theory, $\zeta_n = n/3$. However, experimental investigations (for example Anselmet *et al.* 1984) have revealed that ζ_n exhibits anomalous scaling whereby it deviates from Kolmogorov's linear scaling and instead has nonlinear dependence on n. This anomalous scaling has been attributed to spatial intermittency in the fine structure of the turbulence. Several phenomenological models have been introduced to account for this intermittency, perhaps the most prominent being that of multifractal formalism (for example, see Frisch 1995).

The dissipation range has also long been recognized as being highly intermittent (Batchelor & Townsend 1949) with $\varepsilon(\boldsymbol{x}, t)$ being composed of spatially intermittent regions of high rates of turbulent dissipation. Thus, given that η_K is defined using the mean dissipation rate, it does not reflect the intermittent nature of ε. It is therefore necessary to refine the notion of one mean dissipation length scale to that of a whole continuum of local dissipation scales. One approach is to define a local dissipation scale, η, whereby

$$\eta|\delta_\eta u| \sim \nu \tag{1.4}$$

in which the velocity increment $\delta_\eta u$ is found from (1.3) when $|\boldsymbol{r}| = \eta$ (Paladin & Vulpiani 1987). This is equivalent to identifying instances where the local Reynolds number based on η and $\delta_\eta u$ is unity. This Reynolds number is then also associated with fluid motion at the cross-over scales between the inertial subrange and the viscous dissipation range.

Within the framework of multifractal formalism (Paladin & Vulpiani 1987; Nelkin 1990; Frisch & Vergassola 1991) it has been demonstrated that

$$\eta(h) \sim LRe_L^{-1/(1+h)}, \tag{1.5}$$

where there exists a spectrum of h related to the fractal dimension of their support. The local large-scale Reynolds number $Re_L = \langle|\delta_L u|\rangle L/\nu$ describes the energy containing motions, with $\delta_L u$ defined from (1.3) when $|\boldsymbol{r}| = L$. The Kolmogorov result that $\eta_K \sim LRe_L^{-3/4}$, is recovered for $h = 1/3$; however, a consequence of intermittency is that $h < 1/3$, resulting in the existence of local cross-over scales smaller than η_K.

Biferale (2008) used these foundations to produce an analytical expression for the probability density function (PDF) of η.

An alternative approach to modelling the continuum of dissipation scales was suggested by Yakhot (Yakhot & Sreenivasan 2004, 2005). By letting η_{2n} be an order dependent matching distance between the inertial and dissipative behaviour of $S_{2n}(|\boldsymbol{r}|)$, the scale η_{2n} becomes

$$\eta_{2n} = (\langle [\partial_x u]^{2n} \rangle)^{1/(\zeta_{2n}-2n)} [(2n-1)!! \langle \varepsilon \rangle^{2n/3} L^{(2n/3)-\zeta_n}]^{1/(2n-\zeta_{2n})}. \tag{1.6}$$

This implies that the cross-over scale η is a random field, in that the value of η depends on the order of the structure function being considered. Yakhot & Sreenivasan (2004) found, using the exact equations for the nth-order longitudinal structure functions, that

$$\eta_{2n} \sim LRe_L^{1/(\zeta_{2n}-\zeta_{2n+1}-1)}, \tag{1.7}$$

which recovers the Kolmogorov result when $\zeta_n = n/3$. When combined with (1.4) for $|\boldsymbol{r}| \to \eta$ and assuming

$$\left\langle \left| \frac{\partial u}{\partial x} \right|^n \right\rangle \approx \left\langle \left| \frac{\delta_\eta u}{\eta} \right|^n \right\rangle \tag{1.8}$$

an expression for the Reynolds number dependence of the moments of ε can be found such that

$$\langle \varepsilon^n \rangle \sim Re_L^{d_n}, \tag{1.9}$$

where

$$d_n = n + \frac{\zeta_{4n}}{\zeta_{4n} - \zeta_{4n+1} - 1}. \tag{1.10}$$

Support for this dependence was found within the direct numerical simulation (DNS) results for box and channel flow turbulence (Schumacher 2007; Hamlington *et al.* 2012) and its universality amongst different types of flow recently demonstrated by Schumacher *et al.* (2014) through comparison of the Reynolds number dependence of the moments of ε produced within box, channel flow and Rayleigh–Bérnard convection.

As η is a random field, a description of its PDF is of interest and Yakhot (2006) found an analytical expression describing the PDF of η. When normalized by η_0, this analytic result was found to be in good agreement with the PDFs calculated from the very high-resolution DNS data of three-dimensional homogeneous isotropic box turbulence of Schumacher (2007). The scale η_0 can be considered approximately analogous to η_K (Hamlington *et al.* 2012) and is found from (1.7). To do so, the approximation $\zeta_{2n} = 2an - 4bn^2$ is utilized with $a = 0.383$ and $b = 0.0166$ (Yakhot 2006) giving $\eta_0 = LRe_L^{-1/(1+a-b)} = LRe_L^{-0.73}$. The ratio η_0/η_K is thus expected to be close to unity, increasing slowly as $Re_L^{0.02}$.

PDFs of η/η_0 were also determined experimentally by Bailey *et al.* (2009) in low-Reynolds-number turbulent pipe flow at the centreline and within the upper logarithmic layer. These results were found to be in good agreement with those calculated from homogeneous isotropic DNS, supporting the hypothesis that the form of the PDF, and hence the organization of η, is universal; even for low Reynolds numbers where there is no discernible inertial subrange.

Similar PDFs were also measured by Zhou & Xia (2010) in turbulent Rayleigh–Bérnard convection. However, despite finding good agreement between the PDFs calculated at different locations within the flow and at different Rayleigh number, they

found a higher probability of scales smaller than η_0 compared to Schumacher (2007) and Bailey *et al.* (2009). They attributed this discrepancy to increased intermittency caused by the presence of thermal plumes smaller than η_K.

Recently, Hamlington *et al.* (2012) calculated the PDFs of η/η_0 from DNS results within turbulent channel flow and found that they exhibited strong wall-normal dependence, particularly near the wall. Similar location dependence of the PDF was also observed in free-shear flow by Morshed, Venayagamoorthy & Dasi (2013) who related this spatial dependence to the large-scale shear using a mean-shear Reynolds number. In both studies, the PDFs determined within regions of reduced shear were found to be in agreement with those measured in homogeneous isotropic and nearly homogeneous-isotropic turbulence by Schumacher (2007) and Bailey *et al.* (2009).

These recent results imply that mean shear impacts the distribution of the local dissipation scales, at least at the low Reynolds numbers at which these studies were conducted. Although universality in Reynolds number dependence of $\langle\varepsilon^n\rangle/\langle\varepsilon\rangle^n$ was observed between different flows by Schumacher *et al.* (2014), it was found using data from homogeneous isotropic turbulence, the centreline of channel flow and the centre of the Rayleigh–Bérnard convection cell; locations where mean shear is negligible or minimized. As implied by the assumption of homogeneity and isotropy in the small scales, truly universal behaviour of the small-scale statistics would require that they should also be independent of location within a particular flow.

In the present paper, we experimentally examine the Reynolds number and mean shear dependence of the dissipation moments and η distributions in channel flow and observe that much of the previously observed spatial dependence can be attributed to how the results are normalized. To obtain these statistics we took advantage of recent advances in thermal anemometry and employ a nanoscale thermal anemometry probe (Bailey *et al.* 2010; Vallikivi & Smits 2014) to resolve the small-scale turbulence in the channel flow with sub-Kolmogorov-scale resolution.

2. Experiment description

The experiments were conducted in a turbulent channel flow wind tunnel located at the University of Kentucky. This facility had a channel half-height of $h = 50.8$ mm and could achieve area averaged velocity $U_b = 30$ m s^{-1}, resulting in Reynolds numbers up to $Re_b = 2hU_b/\nu = 1.9 \times 10^5$ or $Re_\tau = hu_\tau/\nu = 4000$, where $u_\tau = (\tau_w/\rho)^{0.5}$ with τ_w the wall shear stress and ρ the density. Air was driven through the channel using an in-line blower located at the inlet with the flow conditioned by a series of six flow conditioning screens and a 9:1 contraction before entering a channel section. The channel section had an aspect ratio of 9:1, expected to provide quasi-2-D flow at the centreline (Zanoun, Durst & Nagib 2003) and was equipped at the channel inlet with a boundary-layer trip consisting of a 50 mm wide section of 120 grit sand paper followed by a 100 mm wide section of 60 grit sandpaper. The distance from the channel inlet to the test location was $246h$, allowing the turbulence to reach a fully developed state naturally (Monty 2005) before entering the measurement section. This measurement section was $24h$ long and was equipped with an insert located at the centre of the upper surface for introducing instrumentation into the flow. Following the measurement section, an additional $12h$ long section isolated the measurement section from exit conditions. Surface roughness was measured on a sample of the measurement section wall using a stylus surface profilometer. The sample was found to have an r.m.s. roughness height of 268 nm along the grain of the aluminium and 334 nm across the grain, corresponding to 2.5 % of the viscous length scale at the highest Reynolds number reported here.

To determine the friction velocity, the channel facility was outfitted with static pressure taps every $12h$ along its length, which allowed determination of the pressure loss in the fully-developed section of the channel using a simple momentum balance (see, for example Pope 2000). For this experiment, the nine pressure taps closest to the measurement section were measured by an array of 1000 Pa transducers. All transducers were calibrated before the experiment using a liquid manometer with ± 0.06 Pa accuracy.

Measurements of streamwise velocity, U_1, were conducted over a range of wall-normal distances, $y = x_2$, at $Re_\tau = 490$, 950, 2080 and 4100. At the lowest Reynolds number, these measurements were made using a conventional hot-wire probe constructed from platinum-core Wollaston wire etched to a sensing length of $\ell = 0.50$ mm and diameter of 2.5 μm. The resulting $\ell^+ = \ell u_\tau/\nu < 5$ with the maximum $\ell/\eta_K \approx 2$ occurring close to the wall. The probe was driven by a constant temperature anemometer (Dantec Streamline CTA) system at an overheat ratio of 1.6 producing a measured square-wave frequency response of $f_{sw} = 60$ kHz. The CTA signal was low pass filtered at 60 kHz using an analogue 4-pole Butterworth filter (Krohn-Hite model 34A) before being digitized at $f_s = 200$ kHz by a 16-bit data acquisition system (National Instruments NI-PCI 6123).

To achieve the higher spatial and temporal resolutions required for the three higher Reynolds number cases, a nanoscale thermal anemometry probe (NSTAP) was used (Bailey & Smits 2010; Vallikivi & Smits 2014). These probes have been successfully employed in the measurement of turbulent wall-bounded flows at both low and high Reynolds numbers (Vallikivi *et al.* 2011; Hultmark *et al.* 2012, 2013; Bailey *et al.* 2014). The probe used in this study had a sensing element measuring 60 μm long × 2 μm wide × 100 nm thick, resulting in $\ell^+ = 1$, 3 and 5 with corresponding maximum $\ell/\eta_K \approx 0.4$, 1.1 and 2.12. The NSTAP was operated in the same system as the conventional probe, although at a resistance overheat ratio of 1.2 which resulted in a square-wave frequency response of $f_{sw} = 120$, 160 and 111 kHz for $Re_\tau = 950$, 2080 and 4100, respectively. Corresponding low-pass filter frequencies were 100, 150 and 100 kHz and digitization frequencies were $f_s = 200$, 300 and 200 kHz.

Calibration of the probes took place *in situ*, directly prior to, and following, each measurement run using a Pitot probe located at the channel centreline. Static pressure was measured by two interconnected 1 mm diameter static taps located 25.4 mm apart, equidistant from the centre plane. To maximize sensitivity over the range of calibration velocities, the pressure difference between Pitot tube and static taps was measured simultaneously by four transducers having sensitivities of 12.5, 125, 750 and 1000 Pa. As with the static taps along the channel length, all transducers were calibrated before the experiment using a liquid manometer with ± 0.06 Pa accuracy. Air temperature was monitored by a thermistor probe located in the measurement section of the channel and CTA bridge voltages corrected in post-processing for any measured temperature drift (Tavoularis 2005). A fourth-order polynomial was used to fit the calibration curves which were used to convert the measured time dependent voltage into time series of U_1.

To traverse the probes in the channel, a nano-stepping traverse equipped with a high-accuracy linear encoder was used (500 nm resolution and ± 3 μm accuracy). The relative position of the hot-wire relative to the wall was set using an electrical contact switch which triggered at the initial probe position for each measurement. The distance of the probe to the wall at this initial measurement location was determined with a distance measuring microscope with an accuracy of ± 5 μm (Titan Tool Supply ZDM-1) and was nominally 85 μm for the hot-wire probe and 50 μm for the NSTAP.

Re_τ	U_b (m s^{-1})	u_τ (m s^{-1})	ν/u_τ (μm)	Probe	ℓ^+	f_{sw} (kHz)	f_s (kHz)	T_sU_b/h	Symbol
490	2.7	0.15	100	HW	5	60	200	21 000	□
950	5.6	0.28	53	NSTAP	1	120	200	43 000	△
2100	14.2	0.64	23	NSTAP	3	160	300	83 900	▽
4100	29.2	1.2	13	NSTAP	5	111	200	34 500	○

TABLE 1. Experimental conditions.

Traverses were made with the number of measurement positions and sample times, T_s, adjusted for each Reynolds number to ensure converged statistics for each case. Experimental conditions are summarized in table 1.

3. Describing the large scales

Within this section we present the measured statistics traditionally used to describe the small scales and use these results to justify the need for a modified descriptor for L in the local large-scale Reynolds number. As typically required for thermal anemometry (i.e. Meneveau & Sreenivasan 1991), Taylor's frozen flow hypothesis (Taylor 1938) was invoked in the calculation of all spatial statistics in order to translate temporal information into spatial information. Here, the local mean streamwise velocity was assumed to be the convective velocity of all turbulent scales such that $\Delta x_1 \approx \langle U_1 \rangle \Delta t$. Although Taylor's hypothesis is generally accepted to be a reasonable approximation for the smallest scales of turbulence, which are the focus of the current study, it is also well known to introduce error in translating the larger scale, long-wavelength motions from the temporal to spatial domain (i.e. Zaman & Hussain 1981; del Álamo & Jiménez 2009).

To estimate η_K an estimate of $\langle \varepsilon \rangle$ must first be found. One approach is to assume local isotropy which allows $\langle \varepsilon \rangle$ to be determined from integration of the one-dimensional dissipation spectrum $D(k_1)$ (Townsend 1976) such that

$$\langle \varepsilon \rangle \approx 15\nu \int_0^{k_c} D(k_1)\,\mathrm{d}k_1 \approx 15\nu \int_0^{k_c} k_1^2 E_{11}(k_1)\,\mathrm{d}k_1. \tag{3.1}$$

Here $D(k_1)$ was, in turn, approximated using the longitudinal one-dimensional energy spectrum $E_{11}(k_1)$ and the streamwise wavenumber found from Taylor's hypothesis using $k_1 \approx 2\pi f/\langle U_1 \rangle$. Since the turbulence signals were oversampled in the present measurements, the integration cutoff k_c was required to prevent contamination of the $\langle \varepsilon \rangle$ estimate by the f^2 noise of the anemometer (Saddoughi & Veeravalli 1996). This cutoff wavenumber was selected using the frequency where an inflection appeared in the frequency spectrum. In other words, the frequency at which instrumentation noise was of the same order as the turbulent signal.

The measured longitudinal one-dimensional energy spectra are shown in figure 1(*a*) for several y positions at each Re_τ with the corresponding one-dimensional dissipation spectra presented in figure 1(*b*). The spectra in figure 1(*a*) have been scaled using Kolmogorov scaling and, as expected, the scaled spectra collapse at large $k_1\eta_K$. Note that, even at the highest Re_τ measured, there is little evidence of the existence of an appreciable inertial subrange. In addition, it was found that for $y^+ = yu_\tau/\nu < 30$ the collapse of the spectra degraded, which is believed to be due to a breakdown in the

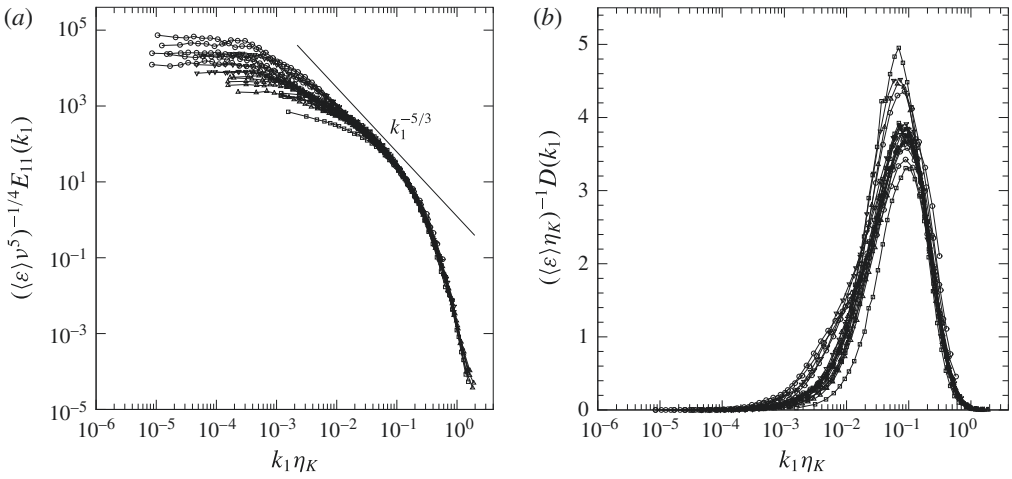

FIGURE 1. (*a*) Normalized longitudinal one-dimensional energy spectra measured at $y^+ \approx 30$ and 100, and at $y/h = 0.2$, 0.5 and 1. (*b*) Corresponding estimate of the dissipation spectra. Symbols as in table 1.

validity of the assumptions used to calculate $\langle\varepsilon\rangle$. For this reason, results from $y^+ < 30$ are not included here.

The wall normal distribution of inner-scaled dissipation $\langle\varepsilon\rangle^+ = \langle\varepsilon\rangle 0.4y/u_\tau^3$ is shown alongside the inner-scaled Kolmogorov scale $\eta_K^+ = \eta_K u_\tau/\nu$ in figure 2(*a*,*b*), respectively. In both cases, the inner-scaled profiles collapse within the range $y^+ < 0.2Re_\tau$, consistent with the dependence of the small-scale properties within the inner layer being dependent only on wall shear stress and viscosity. The collapse within the range $y^+ < 100$ is particularly interesting, given the lack of Reynolds number scaling of the statistics of the large scales for this flow, as reflected, for example, in the growth in the near-wall peak in $\langle u_1^2\rangle^+$ with Re_τ (i.e. as discussed in Marusic *et al.* 2010), but is consistent with the scaling observed by Hutchins *et al.* (2009) in their high-pass filtered streamwise Reynolds stress.

Although the statistics describing the smallest scales follow inner scaling, Reynolds number dependence near the wall can be observed in the Taylor microscale, which here is estimated from

$$\lambda_f \approx \left(\frac{30\nu\langle u_1^2\rangle}{\langle\varepsilon\rangle}\right)^{0.5} \tag{3.2}$$

and shown as profiles of $\lambda_f^+ = \lambda_f u_\tau/\nu$ in figure 2(*c*). Given that λ_f is a hybrid scale formed from a mix of large and small-scale statistics, it is not surprising that the Reynolds number dependence of the large-scale statistics is evident in λ_f^+.

It is often convenient, particularly in homogeneous isotropic turbulence, to characterize the turbulence using the Taylor-scale Reynolds number

$$Re_\lambda = \frac{\lambda_f\langle u_1^2\rangle^{0.5}}{\sqrt{2}\nu}. \tag{3.3}$$

The wall-normal dependence of Re_λ is provided in figure 2(*d*). Whereas at low Re_τ the maximum value of Re_λ occurs near the wall at the location of the near-wall production cycle, as Re_τ increases a local maximum of Re_λ develops in the outer layer near

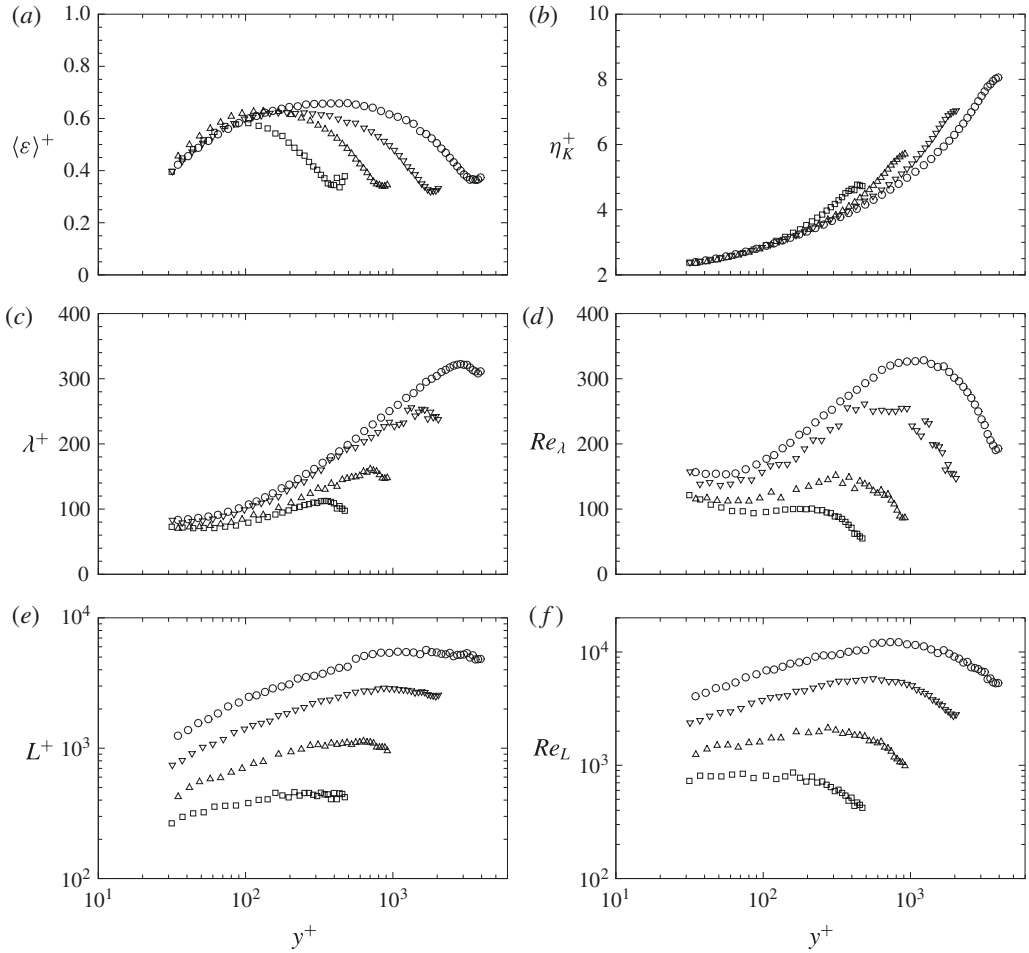

FIGURE 2. Wall normal dependence of: (*a*) mean dissipation rate; (*b*) Kolmogorov scale; (*c*) Taylor microscale; (*d*) Taylor Reynolds number; (*e*) integral length scale; and (*f*) large-scale Reynolds number. Symbols as in table 1.

$y^+ \approx 0.3Re_\tau$. The increase of this outer peak with Re_τ outpaces the near-wall increase in Re_λ with Re_τ. This reflects the increasing confinement in large scales as the near-wall production cycle moves closer to the wall. Thus, even though the turbulence intensity near the wall increases with Re_τ, the increase in turbulence Reynolds number is limited. Conversely, in the outer layer, the large scales remain $O(h)$ and the increase in turbulent kinetic energy production with increasing Re_τ results in a comparatively larger increase in Re_λ compared to near the wall. Note that the non-monotonic wall-normal dependence of Re_λ results in multiple wall-normal locations having identical Re_λ at the same Re_τ.

The integral length scale is commonly used to describe the scale of the energy-containing eddies and is defined from the longitudinal autocorrelation. Here, Taylor's hypothesis is used to find the integral length scale as

$$L = \frac{\langle U_1 \rangle}{\langle u_1^2 \rangle} \int_0^{\tau_c} \langle u_1(t+\tau) u_1(t) \rangle \, \mathrm{d}\tau. \tag{3.4}$$

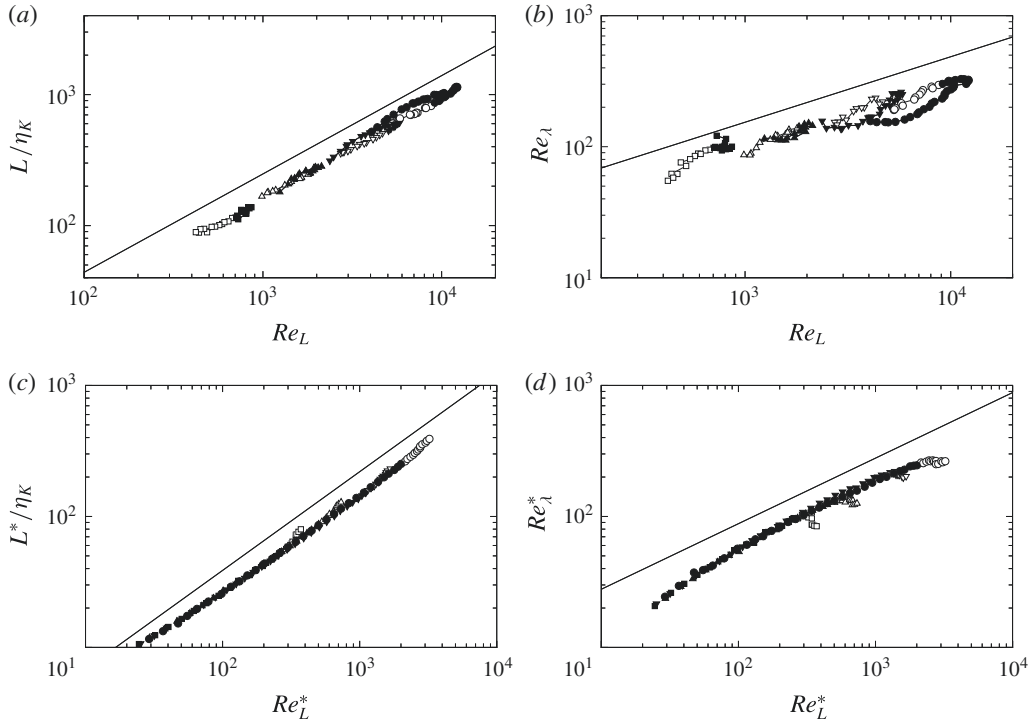

FIGURE 3. Dependence of (*a*) L/η and (*b*) Re_λ on Re_L and dependence of (*c*) L^*/η and (*d*) Re_λ^* on Re_L^*. Symbols as in table 1, solid symbols indicate measurement locations where $y/h < 0.5$.

In practice, small experimental bias and precision errors often result in slow convergence of the integral, so the an upper bound of τ_c was applied. The criterion used here was that of integrating either to the first zero-crossing, or first inflection of the autocorrelation, whichever occurs at a lower value of τ.

The wall-normal dependence of $L^+ = Lu_\tau/\nu$ is presented in figure 2(*e*) and is found to be $O(Re_\tau)$ far from the wall, decreasing towards the wall. The corresponding values of Re_L are shown in figure 2(*f*) and, as with Re_λ, at a single Re_τ there exists multiple y locations with the same value of Re_L. To calculate Re_L, the average velocity increment was estimated by time averaging $|\delta_L u| \approx |u_1(t + L/\langle U_1 \rangle) - u_1(t)|$ for all t.

The non-monotonic wall-normal dependence of the statistics presented in figure 2 reveals the challenge of defining suitable Reynolds number scaling of the small-scale statistics. For example, classical theory suggests $L/\eta_K \sim Re_L^{0.75}$ and $Re_\lambda \sim Re_L^{0.5}$ (see, for example, Frisch 1995). Thus, one would expect Re_λ to have the same value at a certain Re_L, likewise for the ratio L/η_K. However, as shown in figure 3(*a*,*b*), this is not the case. For both figure 3(*a*,*b*) the general trend agrees with the scaling predicted by classical theory. It is also clear that there is both Re_τ and y influence within these trends. It is worthwhile noting that the Re_τ dependence is evident even at relatively high y/h, where the large-scale anisotropy is weak and thus the lack of scaling cannot be attributed to anisotropy of the large scales.

In the phenomenological description of turbulence, the scale L is intended to represent scales at the top of the inertial cascade and have nearly Gaussian statistics.

However it is now understood that the large-scale structure of wall-bounded flow consists of several classes coherent motions. Such motions include the sublayer streaks observed by Kline *et al.* (1967), hairpin vortices in the near-wall region (Head & Bandyopadhyay 1981), low wavenumber large-scale motions which have been associated with the occurrence of bulges of turbulent fluid at the edge of the wall layer (Kim & Adrian 1999; Guala, Hommema & Adrian 2006; Balakumar & Adrian 2007) and meandering, very-large-scale motions or superstructures observed in the overlap region and, for pipes and channel flows, the wake region as well (Kim & Adrian 1999; Tomkins & Adrian 2005; Guala *et al.* 2006; Balakumar & Adrian 2007; Hutchins & Marusic 2007; Monty *et al.* 2007, 2009). In addition, large-scale eddies far from the wall interact with smaller scales near the wall by introducing long wavelength velocity fluctuations through a modulation process (Mathis, Hutchins & Marusic 2009).

Given the complex makeup of the energy containing motions, the integral scale will represent an amalgam of these multiple influences and bias towards longer motions, particularly near the wall, rather than accurately represent eddies with approximately Gaussian statistics at the top of the inertial cascade, as assumed in theoretical treatments (i.e. as done by Yakhot 2006). Thus, it should not be surprising that use of the integral scale for defining Re_L in channel flow is ineffective at capturing the same Reynolds number scaling observed in simpler flows.

Instead, we define a length-scale L^* intended to describe the locally smallest energy-producing (i.e. active) eddies. Correspondingly we can define

$$Re_L^* = \frac{\langle|\delta_L u^*|\rangle L^*}{\nu}, \tag{3.5}$$

$$\lambda_f^* = \left(\frac{30\nu\langle(\delta_L u^*)^2\rangle}{\langle\varepsilon\rangle}\right)^{0.5}, \tag{3.6}$$

and

$$Re_\lambda^* = \frac{\lambda_f^*\langle|\delta_L u^*|\rangle}{\sqrt{2}/\nu}, \tag{3.7}$$

where $\delta_L u^*$ is the longitudinal velocity increment, defined in (1.3), with $|\boldsymbol{r}| = L^*$.

To find L^*, we assume validity of Townsend's attached eddy hypothesis, which states that Reynolds-stress-contributing eddies centred at y are confined by the wall and therefore cannot have a scale larger than y (Townsend 1976). We also note that Perry, Henbest & Chong (1986) hypothesized that the energy containing range of the power spectrum will depend only on u_τ, k_1, y and h given that eddies will only interact if their sizes are comparable. This leads to the assumption that non-local eddies of scale h will contribute only to the low-wavenumber range of the spectrum for $y \ll h$ such that

$$\frac{E_{11}}{u_\tau^2} = g_1(k_1 h) \tag{3.8}$$

and that, following the attached eddy hypothesis, the moderate to high wavenumber portion of the energy-containing range of the spectrum will consist of contributions from eddies scaling with y such that

$$\frac{E_{11}}{u_\tau^2} = g_2(k_1 y). \tag{3.9}$$

Although Perry *et al.* proposed that at sufficiently high Reynolds number an overlap region of validity would exist, leading to a k_1^{-1} scaled subrange, experimental evidence provided by Morrison *et al.* (2004) and Vallikivi, Ganapathisubramani & Smits (2015), amongst others, find little support for this overlap region. However, these studies do demonstrate that within the turbulent wall region ($y/h \lessapprox 0.15$) the low wavenumber portion of the spectrum scales with h and the high wavenumber portion of the spectrum scales with y, as predicted by (3.8) and (3.9). This suggests that the smallest energy-containing eddies, and thus the top of the inertial cascade, is composed of eddies which scale with y. Note also that the largest possible isotropic eddies centred at a given y will have a scale $\propto y$.

We therefore assume that an appropriate length scale to describe the local, active contributions to the Reynolds stress, and upper bound of the inertial subrange, is one that is $\propto y$ for $y \ll h$ which leads to the definition of $L^* = 0.8y$. The constant of proportionality of 0.8 has no theoretical basis but was simply the value found to be most effective at non-dimensionalizing the dissipative motions for $y \lessapprox 0.5h$. However, the results were found to be largely insensitive the constant selected with the greatest sensitivity found in the y dependence of the local dissipation scales presented later in § 5.

It is therefore expected that L^* will result in a value of local-large-scale Reynolds number representing local contributions to Reynolds stress that are free of the non-local, large-scale contributions to velocity fluctuations via amplitude modulation (referred to as 'inactive' eddies by Townsend) which cause L near the wall to be of the same order as h.

The improvement in scaling behaviour through the use of L^* is demonstrated by the dependence of L^*/η and Re_λ^* on Re_L^* as shown in figure 3(*c*,*d*), respectively. In both cases, the agreement with the classical theory is much improved for $y/h < 0.5$, with the Re_τ and y influence on the turbulence parameters in this range captured by the revised description of the large scales. The resulting collapse of the results suggests that Re_L^* is suitable for describing the Reynolds number dependence of the small-scale dissipative statistics in wall-bounded flow, at least for $y/h < 0.5$, where the attached eddy hypothesis can be assumed to be valid.

4. Moments of dissipation rate

As previously noted, through definition of dissipation as a fluctuating field, Yakhot (2006) arrived at (1.9) as a description for the Reynolds number dependence of the moments of the dissipation rate. This theory was tested by Schumacher (2007) using low-Reynolds-number DNS of homogeneous isotropic turbulence and again by Hamlington *et al.* (2012) using DNS of turbulent channel flow. In both cases, good agreement was found with the theory. However, for turbulent channel flow, Hamlington *et al.* (2012) observed that the moments of the dissipation rate exhibited both wall-normal dependence and Re_τ dependence, and thus only the Reynolds number dependence of the nearly isotropic centreline was used to evaluate the exponent n. Therefore, it has yet to be demonstrated that the dissipation rate in the increasingly anisotropic turbulence for $y < h$ follows the predicted scaling.

As the thermal anemometry probe used in the present study was only capable of resolving the streamwise component of velocity, measurement of the all components of the time-dependent local rate-of-deformation tensor was not possible. Hence, the dissipation rate was calculated using the one-dimensional surrogate

$$\varepsilon(t) \approx 15\nu \left(\frac{\partial u_1}{\partial x_1}\right)^2. \tag{4.1}$$

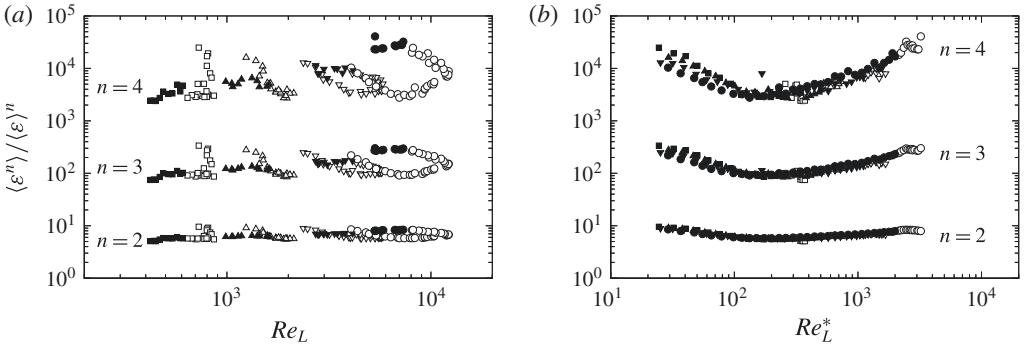

FIGURE 4. (*a*) Normalized dissipation moment. (*b*) Normalized dissipation moments. Symbols as in table 1 with solid symbols in (*a*) indicating measurement locations where $y > 0.6h$ and solid symbols in (*b*) indicating measurement locations where $y < 0.5h$.

As noted by Pope (2000) for example, such surrogates are only assumed to be qualitatively similar to the instantaneous dissipation. Here, to estimate this surrogate, Taylor's hypothesis and a first-order finite difference were employed such that

$$\varepsilon(t) \approx 15\nu \frac{1}{\langle U_1 \rangle^2} \left[\frac{u_1(t + \Delta t) - u_1(t)}{\Delta t} \right]^2 \tag{4.2}$$

with $\Delta t = 1/f_s$. In the present case, to remove contamination from instrumentation noise, an additional zero-phase, eigth-order digital Butterworth filter was applied to the data with a cutoff frequency selected at the frequency at which the spectra is at a local minimum. Estimates of $\langle \varepsilon \rangle$ determined from both (3.1) and (4.2) were found to be in agreement, providing confidence in the implementation of (4.2).

The Reynolds number dependence of the normalized dissipation moments $\langle \varepsilon^n \rangle / \langle \varepsilon \rangle^n$ calculated from the time series determined from (4.2) is shown in figure 4 for $n = 2$–4. When the Reynolds number dependence is examined in terms of the local large-scale Reynolds number using the integral length scale, Re_L, as is done in figure 4(*a*), there is no clear trend in the data, and the Re_τ and y^+ dependence observed in Hamlington *et al.* (2012) is observed. There is also little support for the scaling described by (1.9) in these results.

However, when the Reynolds number dependence of the dissipation moments is expressed using the local large-scale Reynolds number Re_L^*, there is significantly improved collapse of the data amongst the results at different y and Re_τ. For $Re_L^* \lessapprox 200$ the trend is reversed, suggesting insufficient separation between energy-containing and dissipative motions for (1.9) to be valid. Hamlington *et al.* (2012) also observed a similar increase for their lowest Reynolds number case and attributed it to enhanced dissipation introduced by bursting of coherent structures. For $Re_L^* > 200$, the predicted power law behaviour can be observed, at least up to $y/h < 0.8$, which exceeds the limit at which Re_L^* is expected to be a valid descriptor for the large scales. It is expected that as $y \to h$, and the large-scale turbulence becomes increasingly isotropic, L becomes a more suitable descriptor for the large scales. Indeed, as shown in figure 4(*a*) in which data points where $y > 0.6h$ have been highlighted, far from the wall the dissipation moments appear to follow a power law scaling with Re_L. This is coarsely analogous to the inner/outer scaling used to describe the Reynolds

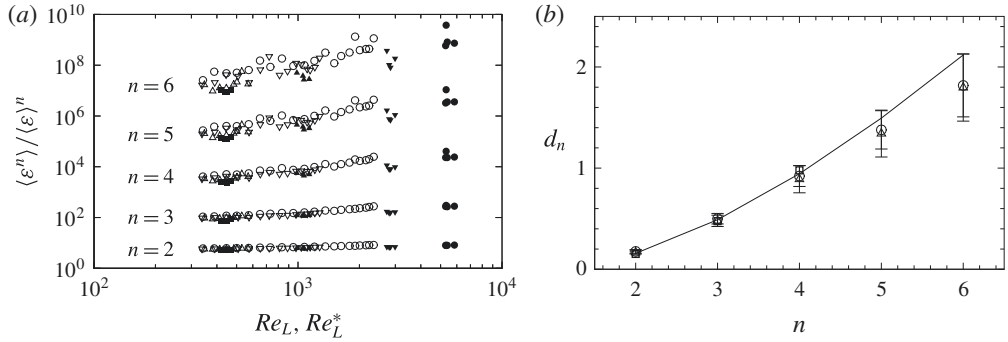

FIGURE 5. (*a*) Normalized dissipation moment data used in the fit to (1.9). Symbols as in table 1 with hollow symbols indicating data points where $y < 0.6h$ and horizontal axis Re_L^* whereas solid symbols indicating data points where $y > 0.8h$ and horizontal axis Re_L. (*b*) Results from fit of (1.9) for $n = 1$–6. Square symbols are the values found by Schumacher *et al.* (2007) from DNS of homogeneous isotropic turbulence, circles are results from the fit using Re_L^* and data points where $y < 0.6h$ and were found to be $d_n = [0.18\ 0.50\ 0.92\ 1.4\ 1.8]$. Triangles are results from the fit using data points using Re_L and $y/ > 0.85h$ and were found to be $d_n = [0.17\ 0.48\ 0.89\ 1.3\ 1.8]$. Solid line (1.9) using (4.3). Error bars represent 90 % confidence level of n estimated from regression analysis.

scaling of the mean flow and, to a lesser extent, the Reynolds stresses, however the ranges in which each form of scaling applies appears to be slightly different in the present case.

To quantitatively compare the Reynolds number dependence to the existing theory, the exponent d_n was determined for $n = 2$–6 by separately fitting (1.9) for the range $Re_L^* > 300$ and $y/h < 0.6$ using Re_L^*, and for the range $y/h > 0.8$ using Re_L. The two sets of data points used in this fit are shown in figure 5(*a*) and the resulting dependence of d_n on n is shown in figure 5(*b*). Also shown in figure 5(*b*) are the homogeneous and isotropic turbulence DNS results of Schumacher, Sreenivasan & Yakhot (2007) and (1.9) with ζ_n estimated using

$$\zeta_n \approx \frac{1.15n}{3(1 + 0.05n)} \tag{4.3}$$

as provided in Yakhot & Sreenivasan (2004). Not only is excellent agreement found between the Re_L^* dependent scaling near the wall and the Re_L dependent scaling in the outer layer but also, for $n \leqslant 4$, with the results of Schumacher (2007) and the theory of Yakhot (2006). Note that the agreement with the theory decreases as n increases, uncertainty in the measured moments decreases, (1.9) requires increasingly higher moments, and the validity of (4.3) decreases. However it is apparent that the present results support the validity of the scaling suggested by (1.9) not only for homogeneous isotropic turbulence but also for anisotropic, channel-flow turbulence, with the caveat that the local large-scale Reynolds number must be suitably defined for the channel-flow case.

5. Scaling of local dissipative scales

As noted earlier, although initial studies of homogeneous or near-homogeneous turbulence (Schumacher 2007; Bailey *et al.* 2009) suggested that the PDFs of η were universal, subsequent investigations in which the PDFs of dissipation scales were

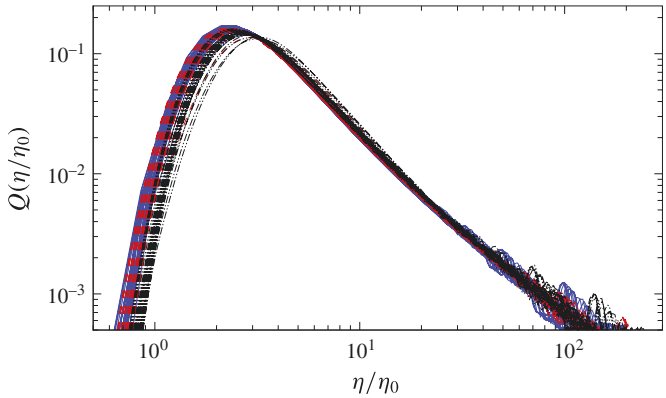

FIGURE 6. (Colour online) Forms of the PDF of local dissipation scales normalized by η_0 for $Re_\tau = 490$, 950 and 2080. Line style indicates Re_τ with dash-dot-dot lines indicating $Re_\tau = 490$, dashed lines indicating $Re_\tau = 950$, and solid lines indicating $Re_\tau = 2080$.

determined in turbulent shear flows (Hamlington *et al.* 2012; Morshed *et al.* 2013) have indicated that they were dependent on the local large-scale shear. However, § 4 demonstrated that when the length scale in the local large-scale Reynolds number is selected to better describe the inertial eddies at the upper bound of the inertial subrange, then the Reynolds number dependence of the dissipation rate better reflects the predicted behaviour within the high shear region near the wall. Here, we investigate the impact that selection of integral scale descriptor has on the scaling of the distribution of local dissipation scales, η.

Following (1.4), the PDF of η represents the probability of an eddy of length scale $r_1 = \eta$ having a local Reynolds number $Re_\eta = |\delta_r u| r_1/\nu \sim 1$. The calculation of the distribution of these scales largely follows that of Bailey *et al.* (2009), whereby the velocity difference at time t is estimated by assuming $r_1 \approx \langle U_1 \rangle \Delta t$ and that $\delta_r u \approx [u_1(t + \langle U_1 \rangle \Delta t) - u_1(t)]$. For a particular discrete measurement time, t, Re_η was calculated over the range $0 < r_1 < 4L$. Each instance where Re_η was between 0.5 and 2 was counted as a single occurrence of dissipation at a scale $\eta = r_1$. This process was performed for all t to generate $Q(\eta)$, the count of occurrences when $0.5 < Re_\eta < 2$ for each value of η. A PDF of η could then be found by normalizing such that

$$\int_0^{4L} Q(\eta)\, \mathrm{d}\eta = 1. \tag{5.1}$$

Note that the integral does not converge as the upper bound increases. It is not clear if this is an artefact of using Taylor's frozen flow hypothesis or a characteristic of the PDF. However, the analytical calculations of the PDF made by Biferale (2008) had power law decay of the large-scale tails, which produced similar behaviour. The PDFs were calculated with unfiltered time series, as well as with the digitally filtered time series used for the analysis in § 4, and were found not to be impacted by the presence or absence of filtering. However, the PDFs at $Re_\tau = 4100$ were found to have insufficient temporal resolution to resolve their small-scale tail and are not included here.

The PDFs calculated from all measurement locations are shown in figure 6 normalized by $\eta_0 = LRe_L^{-0.73}$. The distributions normalized this way are consistent with previously reported distributions determined experimentally, numerically and

analytically. These distributions are highly skewed and characterized by a broad tail stretching into the large scales, a peak near $2\eta_0$ and a much narrower tail at small scales. Also, close inspection of figure 6 shows that the PDFs do not collapse. As also observed in Hamlington *et al.* (2012), there is increasing probability of η/η_0 occurring at larger scales as $y^+ \to 0$. This wall-normal dependence is highlighted in figure 7(*a*,*b*) which better displays the bias towards large scales for $y^+ < 100$, highlighted by the trend in the most probable scale, η_{max}/η_0. However, unlike Hamlington *et al.* (2012), whose investigation was limited to $Re_\tau < 600$, in the present case there is also a slight Re_τ dependence evident.

Thus, when η_0 is used as a scaling parameter, as in figure 7(*a*,*b*), the results suggest non-universality of the small scales and dependence on the large-scale shear (as also suggested by Morshed *et al.* (2013)). Although this non-universality could be attributed to insufficient scale separation at the Reynolds numbers in the present investigation, in the previous sections, L was demonstrated to be an imperfect descriptor for the large scales and hence the normalization parameter η_0 derived from L is also likely to be an imperfect descriptor of the small scales. Instead, following §§ 3 and 4 we define

$$\eta^* = L^* Re_L^{*\,-0.73}. \tag{5.2}$$

The PDFs of η are shown normalized by η^* in figure 7(*c*) for $y/h < 0.5$ and demonstrate greatly improved collapse when compared to figure 7(*a*). Although not evident in figure 7(*c*), some scatter is evident in the small-scale tail of the PDFs normalized by η^* when viewed on logarithmic axes, but it is likely that this scatter is due to experimental error introduced by the stricter temporal resolution requirements which occur as Re_τ increases. Note that the analytical PDF of Biferale (2008) demonstrated Reynolds number dependence in the small-scale tail, although in the form of an increasingly wider tail at higher Reynolds numbers which was the opposite of the behaviour observed in the present results.

The improved collapse when normalized by η^* is highlighted in the wall-normal dependence presented in figure 7(*d*). For $y/h < 0.5$, η_{max}/η^* is constant for all Re_τ with the contours of $Q(\eta/\eta^*)$ also showing much less Re_τ dependence when compared to figure 7(*b*). For $y/h > 0.5$ there is increased Reynolds number dependence in the PDFs as the attached eddy hypothesis used to define L^* becomes increasingly invalid. However, as noted by both Bailey *et al.* (2009) and Hamlington *et al.* (2012), scaling with η_0 results in collapse of the PDFs far from the wall, re-iterating the inner/outer scaling analogy observed in § 4 in which near the wall, the PDFs can be expected to normalize on $\eta^* = f(L^*)$ and far from the wall the PDFs can be expected to normalize on $\eta_0 = f(L)$.

6. Conclusions

Measurements with high temporal and spatial resolution were conducted in turbulent channel flow up to $Re_\tau \approx 4000$ using a nanoscale thermal anemometry probe. The data were used to examine the scaling behaviour of the dissipative range of turbulence. Specifically, through analysis of the Reynolds number dependence of the moments of dissipation rate and the distribution of the dissipative length scales.

In conventional analysis of the small-scale structure, the energetic turbulence is described by a local large-scale Reynolds number, Re_L using length and velocity scales intended to describe the turbulence at the top of the inertial cascade. In practice, this large-scale Reynolds number is often implemented using the local integral length scale of the turbulence. However, it was found that in channel flow

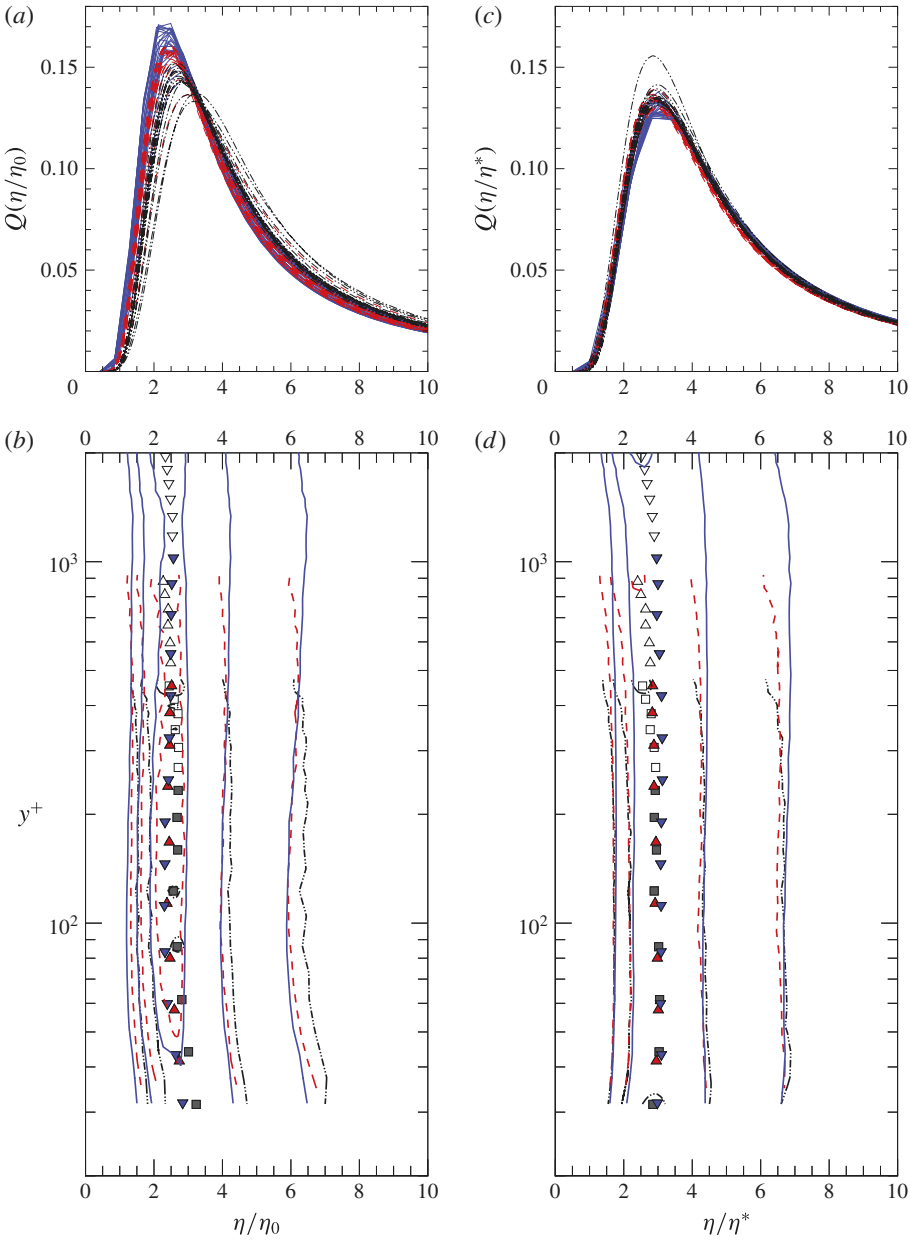

FIGURE 7. (Colour online) (*a*) PDFs of local dissipation scales normalized by η_0 for $y < 0.5h$ from $Re_\tau = 490$, 950 and 2080 and (*b*) isocontours of all PDFs from $Re_\tau = 490$, 950 and 2080 normalized by η_0 showing wall normal dependence. (*c*) PDFs of local dissipation scales normalized by η^* for $y < 0.5h$ from $Re_\tau = 490$, 950 and 2080 and (*b*) isocontours of all PDFs from $Re_\tau = 490$, 950 and 2080 normalized by η^* showing wall normal dependence. Lines indicate Re_τ with dash-dot-dot lines indicating $Re_\tau = 490$, dashed lines indicating $Re_\tau = 950$, and solid lines indicating $Re_\tau = 2080$. Symbols in (*b*,*d*) as in table 1 showing location of maximum probability with filled symbols indicating measurement points where $y < 0.5h$. Contour levels in (*b*,*d*) are spaced 0.025 apart.

the use of the integral length scale to define Re_L resulted in non-unique values of small-scale statistics at a single value of Re_L. This potentially suggests a breakdown of classical scaling, most likely due to the introduction of additional length and velocity scales by the presence of the solid boundary. The non-unique scaling behaviour also runs contrary to the concept of small-scale universality, whereby one would expect the scaling of small-scale statistics to be uniquely defined by the large-scale Reynolds number (as employed as a test of universality by Schumacher *et al.* 2014, for example), and to be independent of location and independent of anisotropy of the large scales.

In wall-bounded flow, where there are both inner-scaled and outer-scaled regions, defining a suitable local Reynolds number for scaling the small-scale statistics is complicated by inner–outer region interactions. Near the wall, these interactions prevent the integral length scale from obeying inner scaling. For example, recent observations have demonstrated that the near-wall turbulence is modulated by large-scale eddies in the outer region. Hence, the integral length scale near the wall will be biased towards larger length scales; reflecting non-local, inactive (i.e. non-Reynolds stress producing) outer-scaled influences.

Within the near wall region, the higher wavenumber bound of the energetic portion of the energy spectrum scales with distance from the wall, which suggests a definition of local large-scale based on distance from the wall, which results in a Reynolds number here referred to as Re_L^*. This Reynolds number represents eddies closer to the top of the inertial cascade and is thus more closely related to the theoretical intent of the local large-scale Reynolds number. Furthermore, this length-scale definition also represents the largest possible isotropic eddies at a given wall-distance.

When the Reynolds number dependence of the small-scale statistics was tested using Re_L^* there was a noticeable improvement in the agreement between the Reynolds number dependence of η_K and λ_f with that predicted for homogeneous isotropic turbulence. The moments of the dissipation rate and distribution of dissipation scales were also found to be better described by Re_L^*, with a clear transition of scaling behaviour observed at $Re_L^* \approx 200$. This transition is consistent with the observations made by Schumacher *et al.* (2014) who noted that small-scale statistics shift away from being Gaussian for $Re > 250$. Schumacher *et al.* also concluded that the small-scale dynamics reach an asymptotic state at this relatively low Reynolds number.

The scaling with Re_L^* degrades in the outer region, where the attached eddy hypothesis loses validity. Instead, in the outer region, as noted by Bailey *et al.* (2009) and Hamlington *et al.* (2012), the small-scale statistics scale with Re_L, suggesting that the dissipation scales follow an inner/outer scaling analogy in which near the wall the dissipation can be expected to be better described by Re_L^* and far from the wall the statistics can be better described by Re_L. It was found that these disparate scaling regions closely follow the traditional inner/outer wall-bounded flow definitions.

Although the results support universality of the small-scale description of turbulence suggested by Yakhot & Sreenivasan (2004, 2005), Yakhot (2006) in high shear turbulence, it should be noted that the revised definition of the local large scale Reynolds number presented here has only been tested in channel flow at relatively low Reynolds numbers. It is not yet clear whether this definition of Re_L^* will hold for other wall-bounded flows, or at higher Reynolds numbers. Furthermore, by definition, Re_L^* is limited to wall-bounded flow. A definition of local large-scale Reynolds number suitable for generalized shear flow is still required to compare the local small-scale statistics between different types of shear flows.

Acknowledgements

This work was supported by Kentucky Science and Engineering Foundation through KSEF-148-502-12-301 and from the National Science Foundation through CBET-1351411. The authors are also grateful to A. Smits, M. Hultmark and M. Vallikivi for providing the NSTAP probes used to conduct the experiments.

REFERENCES

DEL ÁLAMO, J. C. & JIMÉNEZ, J. 2009 Estimation fo turbulent convection velocities and corrections to Taylor's approximation. *J. Fluid Mech.* **640**, 5–26.

ANSELMET, F., GAGNE, Y., HOPFINGER, E. J. & ANTONIA, R. A. 1984 High-order velocity structure functions in turbulent shear flow. *J. Fluid Mech.* **140**, 63–89.

BAILEY, S. C. C., HULTMARK, M., SCHUMACHER, J., YAKHOT, V. & SMITS, A. J. 2009 Measurements of the dissipation scales in turbulent pipe flow. *Phys. Rev. Lett.* **103**, 014502.

BAILEY, S. C. C., KUNKEL, G. J., HULTMARK, M., VALLIKIVI, M., HILL, J. P., MEYER, K. A., TSAY, C., ARNOLD, C. B. & SMITS, A. J. 2010 Turbulence measurements using a nanoscale thermal anemometry probe. *J. Fluid Mech.* **663**, 160–179.

BAILEY, S. C. C. & SMITS, A. J. 2010 Experimental investigation of the structure of large- and very-large-scale motions in turbulent pipe flow. *J. Fluid Mech.* **651**, 339–356.

BAILEY, S. C. C., VALLIKIVI, M., HULTMARK, M. & SMITS, A. 2014 Estimating the value of von Kármán's constant in turbulent pipe flow. *J. Fluid Mech.* **749**, 79–98.

BALAKUMAR, B. J. & ADRIAN, R. J. 2007 Large- and very-large-scale motions in channel and boundary-layer flows. *Phil. Trans. R. Soc. Lond.* A **365**, 665–681.

BATCHELOR, G. K. & TOWNSEND, A. A. 1949 The nature of turbulent motion at large wave-numbers. *Proc. R. Soc. Lond.* A **199**, 238–255.

BIFERALE, L. 2008 A note on the fluctuation of dissipative scale in turbulence. *Phys. Fluids* **20**, 031703.

FRISCH, U. 1995 *Turbulence: The Legacy of A. N. Kolmogorov*. Cambridge University Press.

FRISCH, U. & VERGASSOLA, M. 1991 A prediction of the multifractal model: the intermediate dissipation range. *Europhys. Lett.* **14**, 439–444.

GRANT, H. L., STEWART, R. W. & MOILLIET, A. 1962 Turbulence spectra from a tidal channel. *J. Fluid Mech.* **12**, 241–268.

GUALA, M., HOMMEMA, S. E. & ADRIAN, R. J. 2006 Large-scale and very-large-scale motions in turbulent pipe flow. *J. Fluid Mech.* **554**, 521–542.

HAMLINGTON, P. E., KRASNOV, D., BOECK, T. & SCHUMACHER, J. 2012 Local dissipation scales and energy dissipation-rate moments in channel flow. *J. Fluid Mech.* **701**, 419–429.

HEAD, M. R. & BANDYOPADHYAY, P. 1981 New aspects of turbulent boundary-layer structure. *J. Fluid Mech.* **107**, 297–337.

HULTMARK, M., VALLIKIVI, M., BAILEY, S. C. C. & SMITS, A. J. 2012 Turbulent pipe flow at extreme Reynolds numbers. *Phys. Rev. Lett.* **108**, 094501.

HULTMARK, M., VALLIKIVI, M., BAILEY, S. C. C. & SMITS, A. J. 2013 Logarithmic scaling of turbulence in smooth- and rough-wall pipe flow. *J. Fluid Mech.* **728**, 376–395.

HUTCHINS, N. & MARUSIC, I. 2007 Large-scale influences in near-wall turbulence. *Phil. Trans. R. Soc. Lond.* A **365**, 647–664.

HUTCHINS, N., NICKELS, T. B., MARUSIC, I. & CHONG, M. S. 2009 Hot-wire spatial resolution issues in wall-bounded turbulence. *J. Fluid Mech.* **635**, 103–136.

KIM, K. C. & ADRIAN, R. J. 1999 Very large-scale motion in the outer layer. *Phys. Fluids* **11** (2), 417–422.

KLINE, S. J., REYNOLDS, W. C., SCHRAUB, F. A. & RUNSTADLER, P. W. 1967 The structure of turbulent boundary layers. *J. Fluid Mech.* **30**, 741–773.

KOLMOGOROV, A. N. 1941 The local structure of turbulence in incompressible viscous fluid for very large Reynolds numbers. *Dokl. Akad. Nauk SSSR* **30**, 301–305.

MARUSIC, I., MCKEON, B. J., MONKEWITZ, P. A., NAGIB, H. M., SMITS, A. J. & SREENIVASAN, K. R. 2010 Wall-bounded turbulent flows at high Reynolds numbers: recent advances and key issues. *Phys. Fluids* **22**, 065103.

MATHIS, R., HUTCHINS, N. & MARUSIC, I. 2009 Large-scale amplitude modulation of the small-scale structures in turbulent boundary layers. *J. Fluid Mech.* **628**, 311–337.

MENEVEAU, C. & SREENIVASAN, K. R. 1991 The multifractal nature of turbulent energy dissipation. *J. Fluid Mech.* **224**, 429–484.

MONTY, J. P. 2005 Developments in smooth wall turbulent duct flows. PhD thesis, University of Melbourne.

MONTY, J. P., HUTCHINS, N., NG, H. C. H., MARUSIC, I. & CHONG, M. S. 2009 A comparison of turbulent pipe, channel and boundary layer flows. *J. Fluid Mech.* **632**, 431–442.

MONTY, J. P., STEWART, J. A., WILLIAMS, R. C. & CHONG, M. S. 2007 Large-scale features in turbulent pipe and channel flows. *J. Fluid Mech.* **589**, 147–156.

MORRISON, J. F., MCKEON, B. J., JIANG, W. & SMITS, A. J. 2004 Scaling of the streamwise velocity component in turbulent pipe flow. *J. Fluid Mech.* **508**, 99–131.

MORSHED, N. M., VENAYAGAMOORTHY, S. K. & DASI, L. P. 2013 Intermittency and local dissipation scales under strong mean shear. *Phys. Fluids* **25**, 011701.

NELKIN, M. 1990 Multifractal scaling of velocity derivatives in turbulence. *Phys. Rev.* A **42** (12), 7226–7229.

PALADIN, G. & VULPIANI, A. 1987 Degrees of freedom of turbulence. *Phys. Rev.* A **35**, 1971–1973.

PERRY, A. E., HENBEST, S. & CHONG, M. S. 1986 A theoretical and experimental study of wall turbulence. *J. Fluid Mech.* **165**, 163–199.

POPE, S. B. 2000 *Turbulent Flows*. Cambridge University Press.

SADDOUGHI, S. G. & VEERAVALLI, S. V. 1994 Local isotropy in turbulent boundary layers at high Reynolds number. *J. Fluid Mech.* **268**, 333–372.

SADDOUGHI, S. G. & VEERAVALLI, S. V. 1996 Hot-wire anemometry behaviour at very high frequencies. *Meas. Sci. Technol.* **7**, 1297–1300.

SCHUMACHER, J. 2007 Sub-Kolmogorov-scale fluctuations in fluid turbulence. *Europhys. Lett.* **80**, 54001,1–6.

SCHUMACHER, J., SCHEEL, J. D., KRASNOV, D., DONZIS, D. A., YAKHOT, V. & SREENIVASAN, K. R. 2014 Small-scale universality in fluid turbulence. *Proc. Natl Acad. Sci. USA* **111**, 10961–10965.

SCHUMACHER, J., SREENIVASAN, K. R. & YAKHOT, V. 2007 Asymptotic exponents from low-Reynolds-number flows. *New J. Phys.* **9**, 89.

TAVOULARIS, S. 2005 *Measurement in Fluid Mechanics*. Cambridge University Press.

TAYLOR, G. I. 1938 The spectrum of turbulence. *Proc. R. Soc. Lond.* A **164** (919), 476–490.

TOMKINS, C. D. & ADRIAN, R. J. 2005 Energetic spanwise modes in the logarithmic layer of a turbulent boundary layer. *J. Fluid Mech.* **545**, 141–162.

TOWNSEND, A. A. 1976 *The Structure of Turbulent Shear Flow*. Cambridge University Press.

VALLIKIVI, M., GANAPATHISUBRAMANI, B. & SMITS, A. J. 2015 Spectral scaling in boundary layers and pipes at very high Reynolds numbers. *J. Fluid Mech.* **771**, 303–326.

VALLIKIVI, M., HULTMARK, M., BAILEY, S. C. C. & SMITS, A. J. 2011 Turbulence measurements in pipe flow using a nano-scale thermal anemometry probe. *Exp. Fluids* **51**, 1521–1527.

VALLIKIVI, M. & SMITS, A. J. 2014 Fabrication and characterization of a novel nanoscale thermal anemometry probe. *J. Microelectromech. Syst.* **23** (4), 899–907.

YAKHOT, V. 2006 Probability densities in strong turbulence. *Physica* D **215** (2), 166–174.

YAKHOT, V. & SREENIVASAN, K. R. 2004 Towards a dynamical theory of multifractals in turbulence. *Physica* A **343**, 147–155.

YAKHOT, V. & SREENIVASAN, K. R. 2005 Anomalous scaling of structure functions and dynamic constraints on turbulence simulations. *J. Stat. Phys.* **121**, 823–841.

ZAMAN, K. B. M. Q. & HUSSAIN, A. K. M. F. 1981 Taylor hypothesis and large-scale coherent structures. *J. Fluid Mech.* **112**, 379–396.

ZANOUN, E. S., DURST, F. & NAGIB, H. 2003 Evaluating the law of the wall in two-dimensional fully developed turbulent channel flows. *Phys. Fluids* **15**, 3079–3089.

ZHOU, Q. & XIA, K.-Q. 2010 Universality of local dissipation scales in buoyancy-driven turbulence. *Phys. Rev. Lett.* **104**, 124301.